

Non-Destructive Optical Techniques for the Detection of Defects and Stress in Sapphire

Ikerionwu A. Akwani, Douglas L. Hibbard, Keith T. Jacoby

Exotic Electro-Optics (EEO), 36570 Briggs Road Murrieta, California, 92563

Abstract

Because of its high strength and wide practical wavelength range, sapphire has become the material of choice for large aperture windscreens for a number of electro-optical system applications. Surface stress, sub-surface damage and bulk stress introduced during crystal growth and optical fabrication can each deleteriously effect critical opto-mechanical performance characteristics in windows such as strength and durability. Traditional methods for measuring these defects are destructive and, therefore, unsuitable as in-process inspection tools for actual flight hardware. Several non-destructive optical techniques are presently under investigation at Exotic Electro-Optics under funding by the Air Force Research Laboratory. These include polarization-based methods. An update on experimental results using the photoelasticity technique, a modified circular polariscope, will be presented. The ultimate goal of this research program is to provide a better understanding of the overall manufacturing process leading to the optimal fabrication process parameters, time and cost.

1.0 Introduction

Crystal growth and optical fabrication processes such as grinding and polishing operations lead to the creation of surface and sub-surface damage. These defects degrade the strength and the performance of functional materials. In order to optimize thermo-mechanical performance, the damaged layer must be identified and minimized or eliminated by subsequent process steps.

Traditional testing methods for measuring surface stress and sub-surface damage include ball indentation testing, cleaving and cross-sectional analysis, and wedge-polish-etch testing, which are all destructive tests [1, 2, 3]. The basic goal of this study is to identify and develop a method capable of detecting and quantifying defects, stress and sub-surface damage using a non-destructive approach. More specifically, this work is focused on a polarization-based method (photoelasticity) that appeared to be the most applicable as a large sapphire panel stress and defect mapping tool.

To evaluate the application of this non-contact technique to the detection of defects and stress fields inherent or applied to sapphire panels, a set of a-plane sapphire panels were characterized. The sample set was composed of a number of polished specimens. The stress fields occurring in a sapphire crystal panel are caused by the distortion of the crystal lattice. Our objective in this set of experiments was two-fold: (a) to use a modified polariscope to detect defects in sapphire panels and (b) to investigate the stress pattern/distribution associated with applied loads and begin to quantify those effects.

2.0 Optical birefringence (retardation)

Optical polarization based methods are well established means of characterizing materials. In this case, the technique involves measuring the relative retardance of two orthogonal linearly

polarized light rays (n_e and n_o are the refractive indices of the extraordinary and ordinary rays) as they pass through a sapphire panel. The beam emerging from the panel is transformed into circular, elliptical or linear polarization state depending on the value of the induced phase shift. The index of refraction of the n_e ray varies with the direction of light propagation as follows:

$$n_{e(\theta)} = \frac{n_e n_o}{\sqrt{\{(n_e^2 \cos^2 \theta) + (n_o^2 \sin^2 \theta)\}}} \quad (1)$$

where θ is the angle between direction of the beam and the optical axis. Birefringence, $(n_e - n_o)$, will be maximum when the extraordinary ray is perpendicular to the optical axis. This yields the highest degree of interference coloration. Figure 1 shows the index surface of an optically uniaxial crystal for a positive and negative crystal.

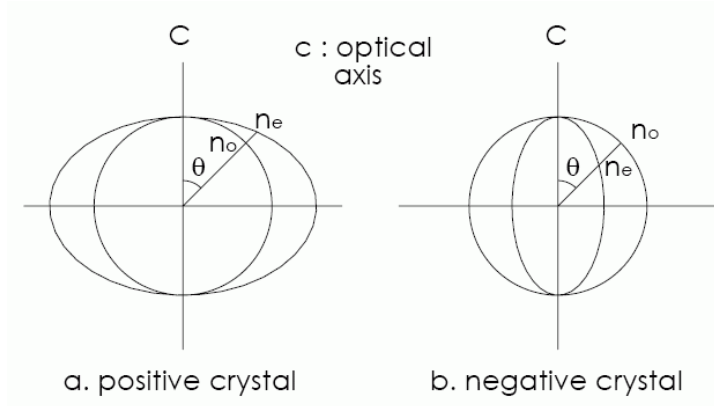


Figure 1. (a) and (b) index surface of an optically uniaxial crystal where θ is the angle between direction of the beam and the optical axis.

Birefringence is also sensitive to the stress state of the material. As such, the measured level of birefringence can be used to quantify stress in the panel. The relationship between retardance and birefringence is given by

$$\text{retardation} = h(n_e - n_o) \quad (2)$$

and the corresponding phase difference is

$$\Delta = \frac{2\pi h}{\lambda_0} (n_e - n_o) \quad (3)$$

where h is the thickness of the sapphire panel in nanometers and λ_0 is the vacuum wavelength. The phase difference or relative retardation, Δ , of the emergent beams is related to the principal-stress difference, $(\sigma_1 - \sigma_2)$, using the Stress-Optic law, as follows:

$$\Delta = \frac{2\pi h c}{\lambda} (\sigma_1 - \sigma_2) \quad (4)$$

where λ is the wavelength of light used and c is the direct stress-optic coefficient. The relative retardation changes from point to point depending on the degree of stress. Therefore, the intensity of light transmitted is governed by the stress fields. The relationship between the transmitted light intensity and relative retardation, Δ , or principal stress difference, $(\sigma_1 - \sigma_2)$, for a circular polariscope is given as:

$$I = I_0 \sin^2 \frac{\Delta}{2} \quad (\text{for dark-field}) \quad (5)$$

$$I = I_0 \cos^2 \frac{\Delta}{2} \quad (\text{for bright-field}) \quad (6)$$

where I and I_0 are the output intensity and incident intensity, respectively. It is convenient to express equation (4) as

$$\sigma_1 - \sigma_2 = \frac{K f_\sigma}{h} \quad (\text{N/m}^2) \quad (7)$$

where K is the relative retardation in terms of a complete cycle of retardation,

$$K = \frac{\Delta}{2\pi} \quad (8)$$

and

$$f_\sigma = \frac{\lambda}{C} \quad (9)$$

is the material fringe value. For a given material fringe value, f_σ , and relative retardation, K , the principal-stress difference $(\sigma_1 - \sigma_2)$ can be determined at every point. Practically, K (the measured fringe order) is determined with a polariscope and f_σ is established by calibration techniques.

By using appropriate combinations of wave-plates (quarter and half wave plates) and coordinating their orientations with respect to the optical axis, any desired output polarization state can be achieved. This provides the basis for applications to support material characterization and product development.

3.0 Experimental Set-Up and Results

The basic optical set-up for the experiment reported here is a circular polariscope incorporating an additional birefringent plate, as shown in Figure 2. In general, the instrument consists of an assembly of optical components such as rotating waveplate/retarders and polarizers, a white light and a CCD detector.

The samples used for this study were a-plane sapphire, grown by the Edge-defined Film-fed Growth (EFG) technique. During growth, the crystal is pulled from the melt along the m-axis as shown in Figure 3. Using a conventional circular polariscope configuration, the signal from defects/birefringence is very weak and practically undetectable. In order to readily detect defects in sapphire, an extra birefringent plate for amplification must be incorporated as shown. Figure 4 shows a collection of images of sapphire panels obtained using the polariscope diagrammed in Figure 2. The photographs in Figure 4 fundamentally illustrate the use of modified cross-polarizers in the qualitative analysis of defects in sapphire panels.

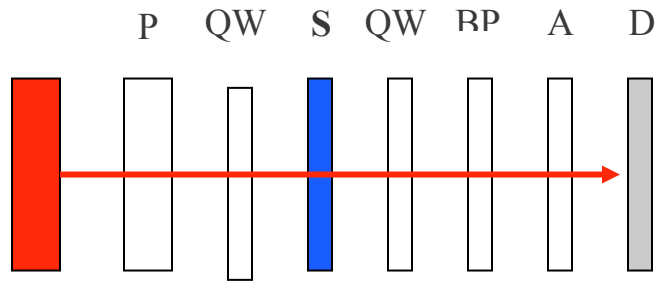


Figure 2. Basic experimental set-up: P= polarizer, QW=quarter waveplate, S= sapphire panel, BP= birefringent plate, A= analyzer and D= detector/CCD camera.

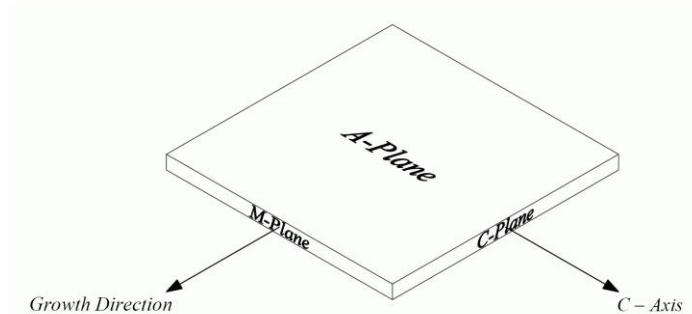


Figure 3. Schematic diagram of the crystal orientations of a-plane sapphire used in the study.

Figure 4(a) was obtained without the additional birefringent plate. As can be seen, no visible defect is observed. The incorporation of the extra birefringent plate results in the enhanced visibility of defects as shown in Figure 4(b). In this case, the defect consists of striations which are observed to run perpendicular to the direction of material growth, namely along the m-axis (10-10) of the sapphire crystal.

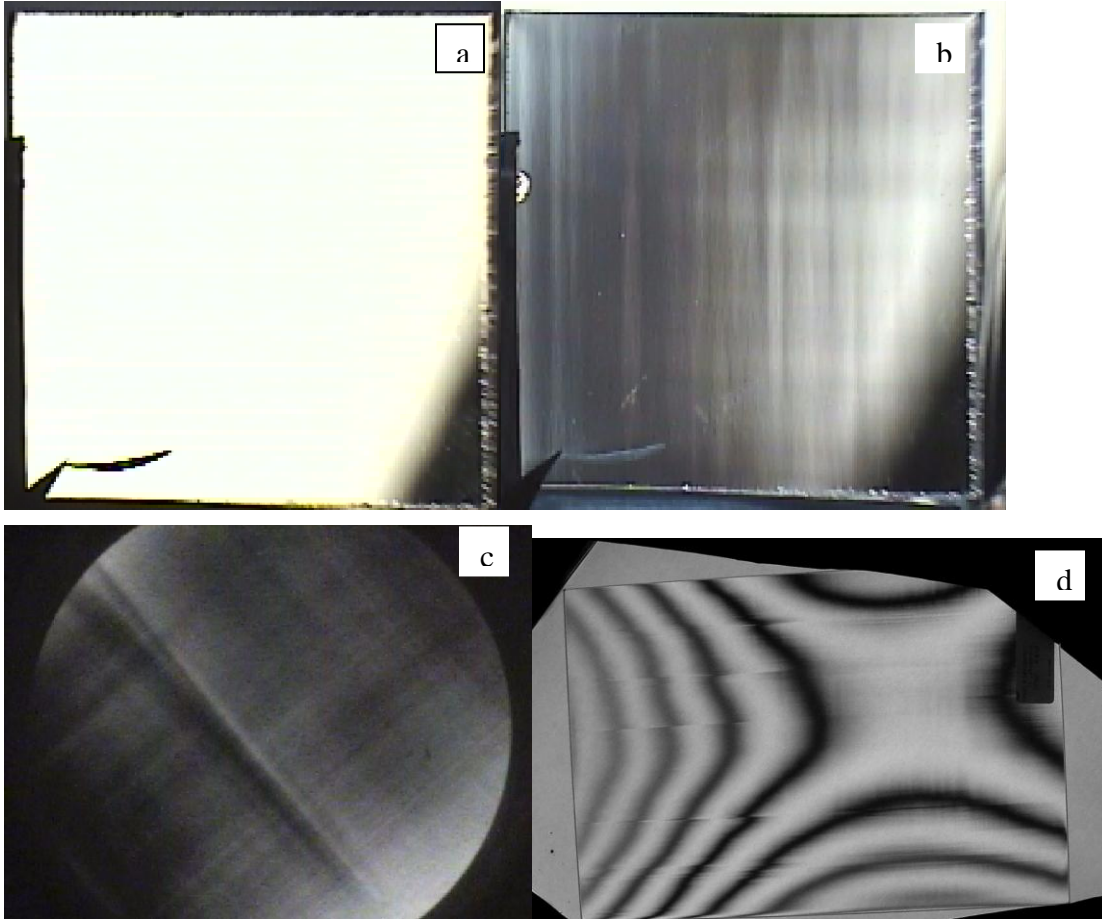


Figure 4. (a) Sapphire panel 1 without the additional plate exhibiting no sign of defects; (b) sapphire panel 1 with the extra plate now exhibiting growth-related striations; (c) sapphire panel 2 showing growth defects and lattice distortions; (d) sapphire panel 3 showing growth defects and fringes associated with stress.

The observed defects are attributed to growth-induced inhomogeneities that may affect the processing and end-application of the sapphire panel. Figure 4(c) exhibits growth defects in addition to lattice distortion that are each clearly visible. This distortion is characterized by a ridge-like structure that appears to split into two. Superimposed on this feature are small lines running perpendicular to it. This particular feature has been observed previously in other sapphire panels and it is attributed to the growth process. However, the origin of the ridge-like structure is difficult to ascertain from the present study since no baseline data from the panel in the as-received state were obtained prior to processing.

In Figure 4(d), growth defects and fringes associated with stress are observed. Since stress fields in crystals change the electron density and the indices of refraction are mainly determined by electron density, it follows that the observed striations and lattice distortions show varying indices of refraction in different regions of the sapphire panel. Again, the detection of these defects is improved by the extra birefringent plate.

Figure 5 shows the effect of analyzing beam direction versus the sapphire c-axis. In general, the results show significant differences in defect visibility and interference colors. For example, defects appear to be fainter and more colorful with increasing angle. For rotation angles of less than 10 degrees, defects are more visible. Between 12 and 40 degrees, broad interference color

dominates with no defects visible. These results might be explained on the basis of Figure 1 above, and the results suggest the criticality of optical alignment in defect detection.

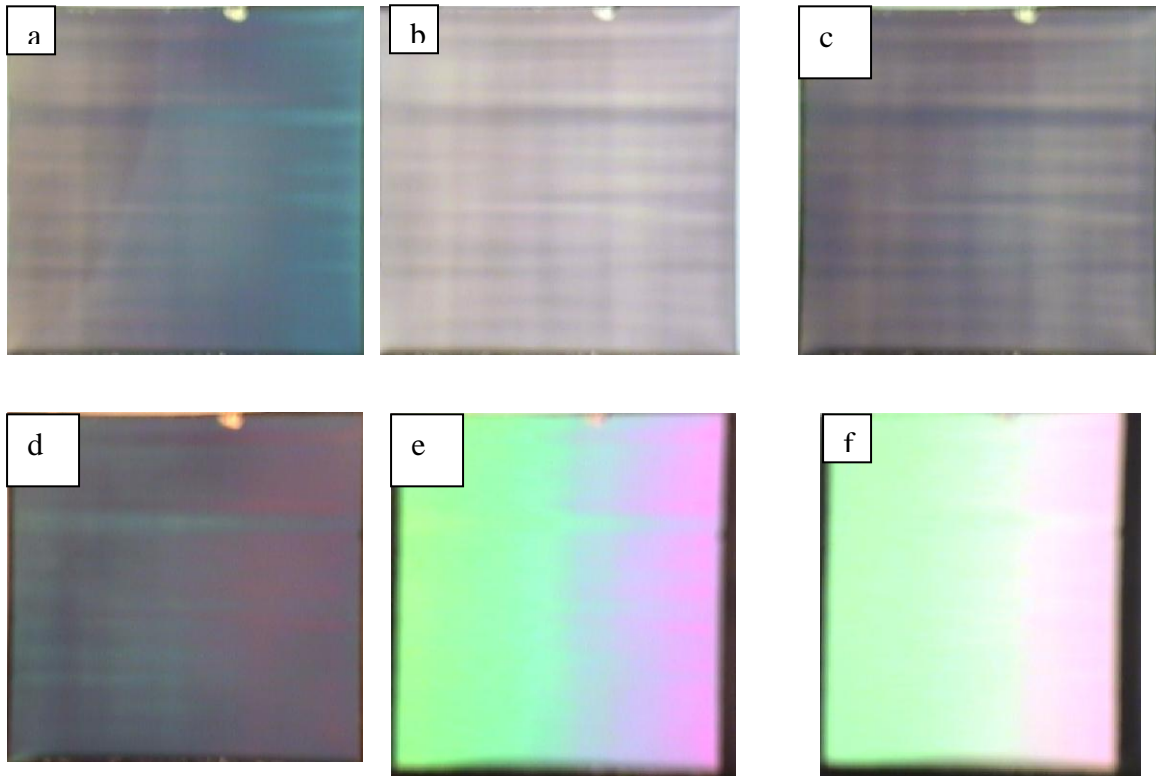


Figure 5. Images show the effect of analyzing beam direction versus the sapphire c-axis. (a) Image taken at 0 degrees difference; (b) image taken at 6 degrees difference; (c) image taken at 10 degrees difference; (d) image taken at 12 degrees difference; (e) image taken at 30 degrees difference; (f) image taken at 40 degrees difference.

Similarly, Figure 6 shows the effect of the analyzing beam direction versus the sapphire m-axis. In general, the defects get fainter and the sapphire changes both in color and intensity with rotation around this axis. At angles less than 10 degrees, the defects are visible. At 12 degrees, no defects are observed and the image appears black indicating that no light is transmitted through the crossed polarizers. Between 15 and 20 degrees, defects are barely visible and colors begin to develop. Between 25 and 40 degrees, broad interference colors are observed with no visible defects. At 30 to 40 degrees, the colors appear more uniform.

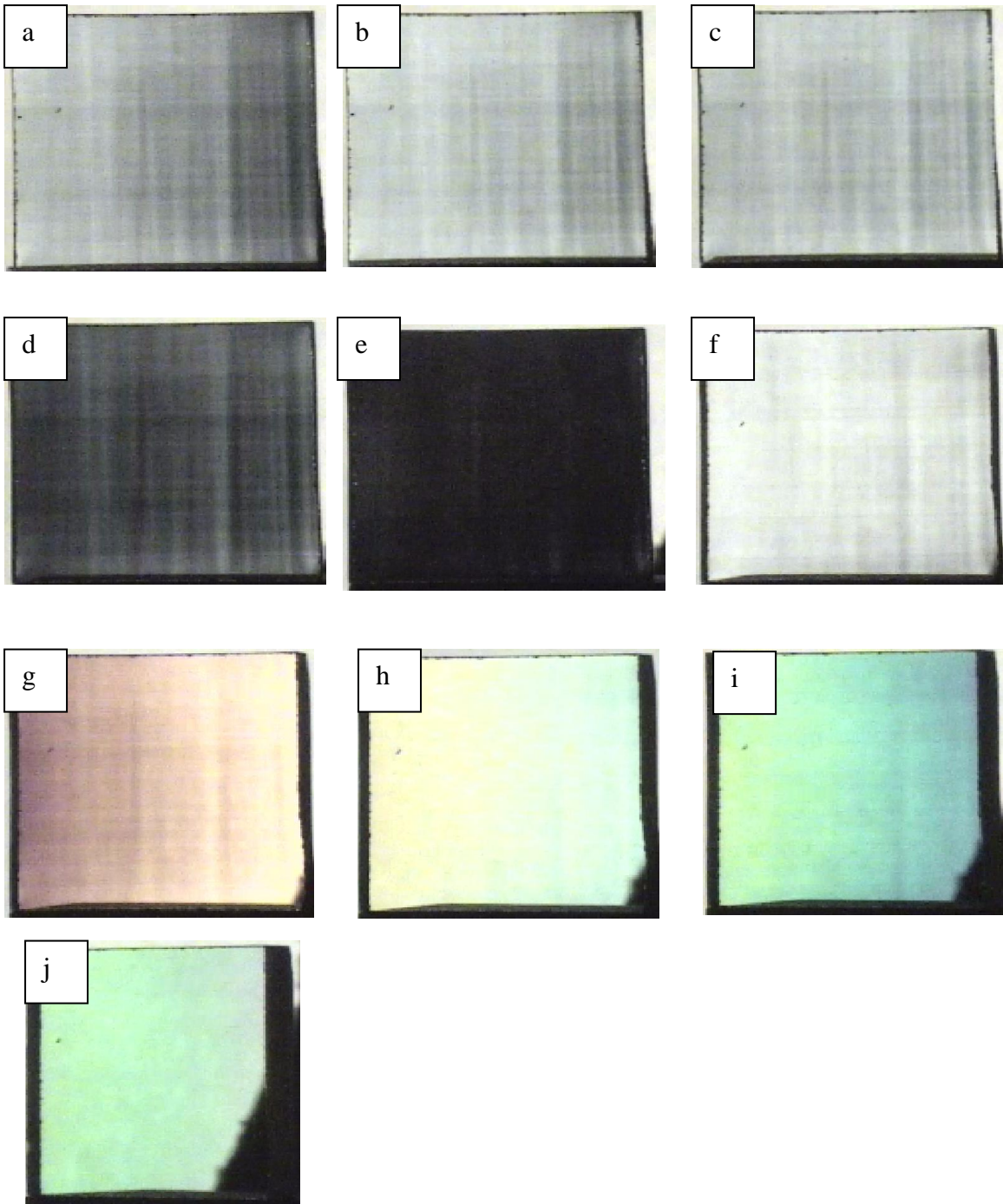


Figure 6. Images show the effect of analyzing beam direction versus the sapphire m-axis. (a) Image taken at 0 degrees difference; (b) image taken at 2 degrees difference; (c) image taken at 6 degrees difference; (d) image taken at 10 degrees difference; (e) image taken at 12 degrees difference; (f) image taken at 15 degrees difference; (g) image taken at 20 degrees difference; (h) image taken at 25 degrees difference; (i) image taken at 30 degrees difference; (j) image taken at 40 degrees difference.

In Figure 7 the effect of polarization angle on defect detection is illustrated. Images were taken for angles of 30, 70, 90, 110 and 140 degrees between the polarizer and analyzer axes. It is clear from the figure that defect visibility depends on the polarization direction. Defects appear fainter with increasing polarization angle. At 140 degrees, defects become almost undetectable.

Figures 8 and 9 show the evolution of stress distribution in a sapphire panel with applied load. Uniaxial stress was applied via a calibrated mechanical clamping mechanism along the m-direction (Figure 9) and the c-direction (Figure 8). The spatial variation of the stress field was obtained by imaging the light transmitted through the sample during the uniaxial compression. From the figures, one can see significant differences in the images as a function of applied stress and sample orientation. In general, mixed regions of dark and bright areas are clearly observed. The color variation shows the signal strength and the bright areas indicate higher internal stress.

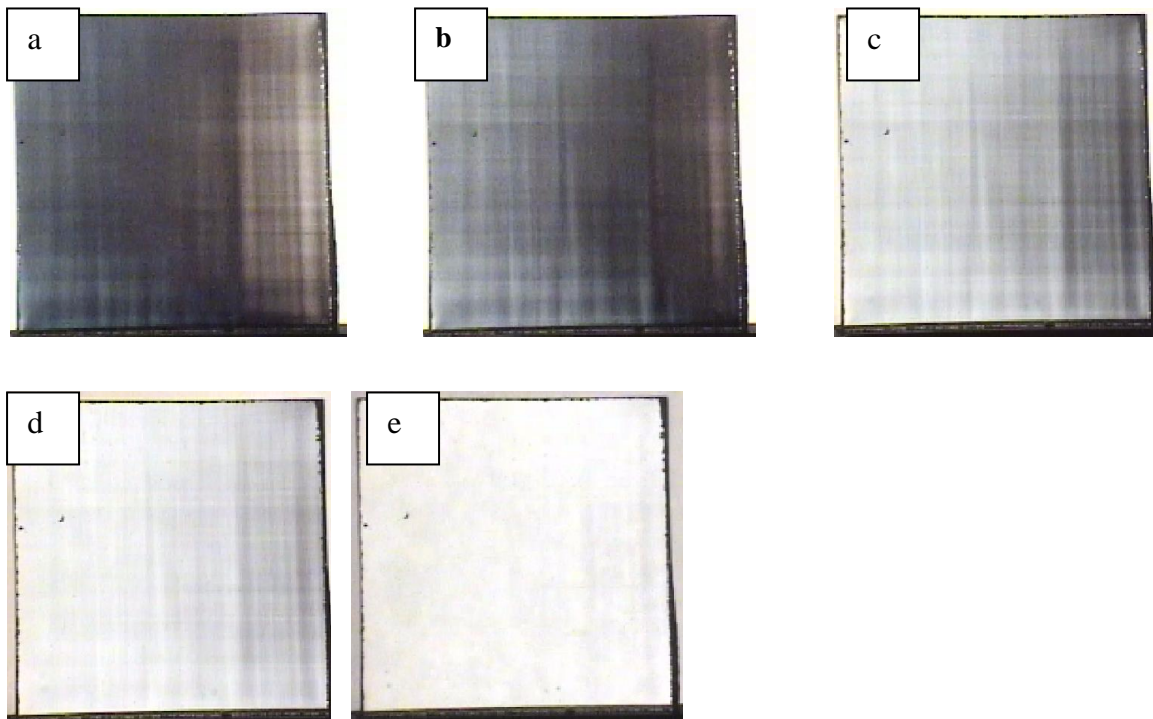


Figure 7. Images show the effect of polarization angle on defect detection. (a) Image taken at 30 degrees; (b) image taken at 70 degrees; (c) image taken at 90 degrees; (d) image taken at 110 degrees; (e) image taken at 140 degrees.

By comparing the image in the zero applied stress state and 5-pound stressed state, it is apparent that the dark areas at zero applied stress become the bright areas in the stressed image and vice versa. This change indicates a change in retardation value associated with the applied stress. The change in phase difference over the same physical path length in sapphire is also increased as the applied load is increased; hence, an increase in deformation corresponds to an increase in bright areas. The bright areas are due to the stress-induced refractive index change which is related to the phase shift by equation (3) above. Regions of highest induced local stress (stress concentration points) are clearly visible (colored regions). As the applied load is increased, the stress concentration points increase toward the center of the panel.

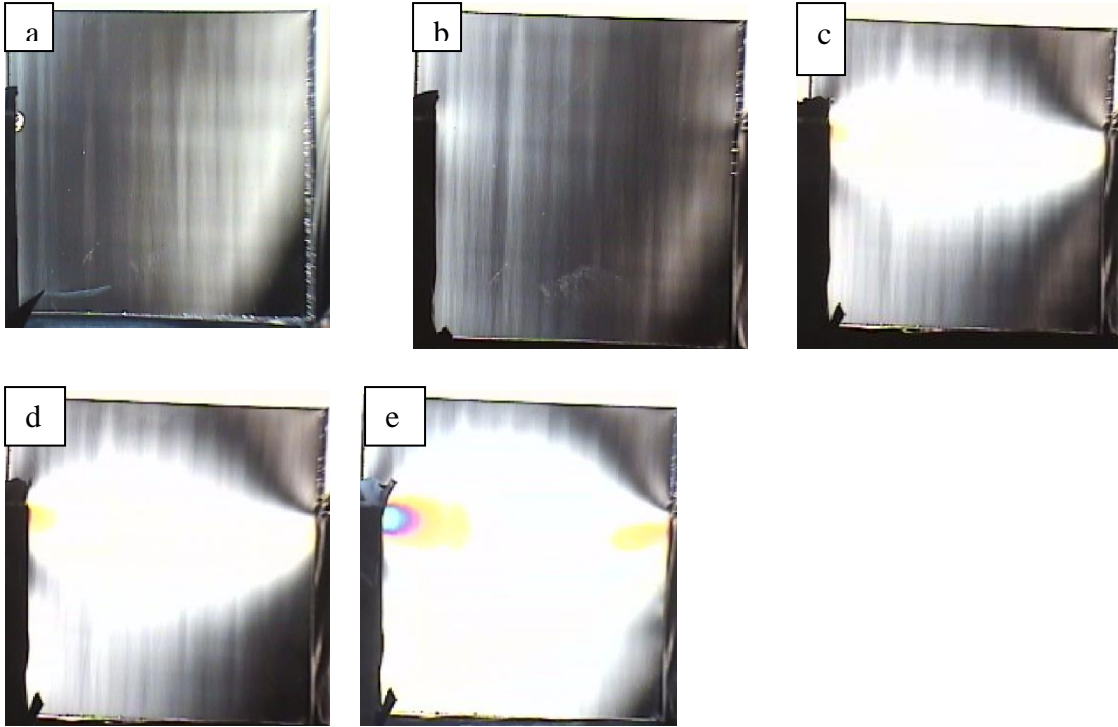


Figure 8. Images show the effect of applied load on the apparent stress distribution in the panel. (a) Image taken with zero applied stress; (b) image taken with 5 lbs of applied stress; (c) image taken with 10 lbs of applied stress; (d) image taken with 13 lbs of applied stress; (e) image taken with 19 lbs of applied stress.

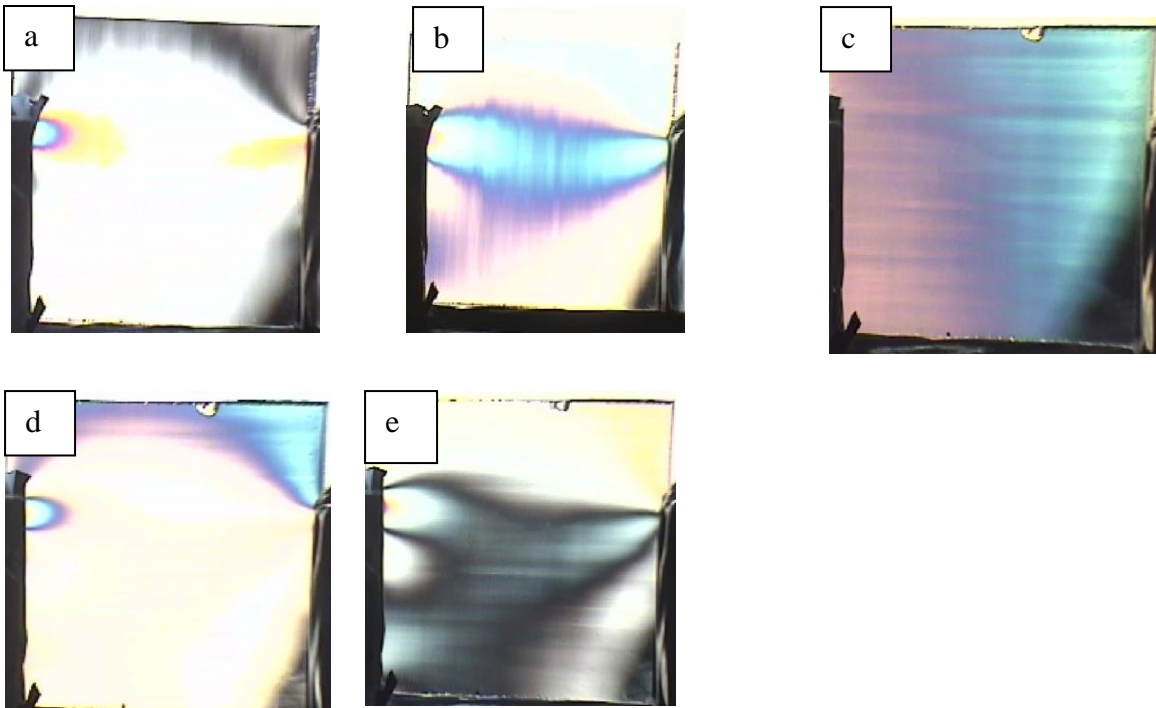


Figure 9. Images show the effect of applied load on the apparent stress distribution in the panel. (a) Image taken with 24 lbs of applied stress in dark-field mode; (b) image taken with 24 lbs of applied stress in light-field mode; (c) image taken with 5 lbs of applied stress, sample rotated 90 degrees, in bright-field mode; (d) image taken with 20 lbs of applied stress, sample rotated 90 degrees, in bright-field mode; (e) image taken with 20 lbs of applied stress in dark-field mode.

Existing material defects are strongly affected by the application of induced stress, as illustrated by the brightness of the defect line (growth striation) in the dark-field mode in Figure 8 and Figure 9(a). This type of defect may act as a stress amplifier, creating preferred sites for crack initiation, resulting in overall strength degradation of the sapphire panel. Interestingly, this might in part explain the variability in strength observed in sapphire panels. The observation of a stress gradient across the panel suggests that atomic motion is parallel to the direction of uniaxial compression. As the material is deformed, the material-light interactions change. The material's microscopic atomic rearrangement or behavior under applied stress leads to a change in the macroscopic electric polarization of the material. The index of refraction varies with the polarizability of the bonds in the material. The light intensity is a function of the index of refraction which in turn depends on the magnitude of the applied stress.

The representative stress distributions of four inspection-polished sapphire panels are shown in Figure 12. This is the condition of panels as-received from the crystal growth vendor. This figure clearly shows stress-induced multicolored regions in the sapphire panels. The observed interference colors stem from the wavelength dependence of the retardation as described above. If the retardance varies from one region to the next across the sapphire panel, the color of the light transmitted will vary correspondingly. The observed colors represent varying stress levels. In general, all four sapphire panels exhibit a similar characteristic stress pattern which includes a saddle point close to the center of the panel. These saddle-shaped stress distributions are common in photoelastic measurements. The stress/fringe pattern is not symmetric about the saddle point in each case. The density of fringes throughout the sapphire panel indicates the degree of stress variation. Comparison of the sapphire panels show that the exact shape of the saddle point and the number of fringes in each panel is different, therefore indicating a different value of stress for each panel. As the stresses increase, the fringe bands become narrower, denser and closely spaced due to phase differences as described above in equation (4). This implies that the right of the saddle point exhibits the highest stress value since it contains the greatest density of fringes, followed by the left side, above and below the saddle point for Figure 12 (a), (b) and (c) while for (d) the order of decreasing stress is right, above, left and below. In addition, a close examination of Figure 12 (b), (c) and (d) reveals evidence of other defects as indicated by the arrows. These results demonstrate the capability of the photoelastic technique to detect stresses and defects on large sapphire panels very early in the fabrication process.

It is important to clarify that in order to quantitatively characterize stress in sapphire panels one needs to determine the photoelastic constant, f_{σ} (which is a material dependent quantity), and use equation (7), as described.

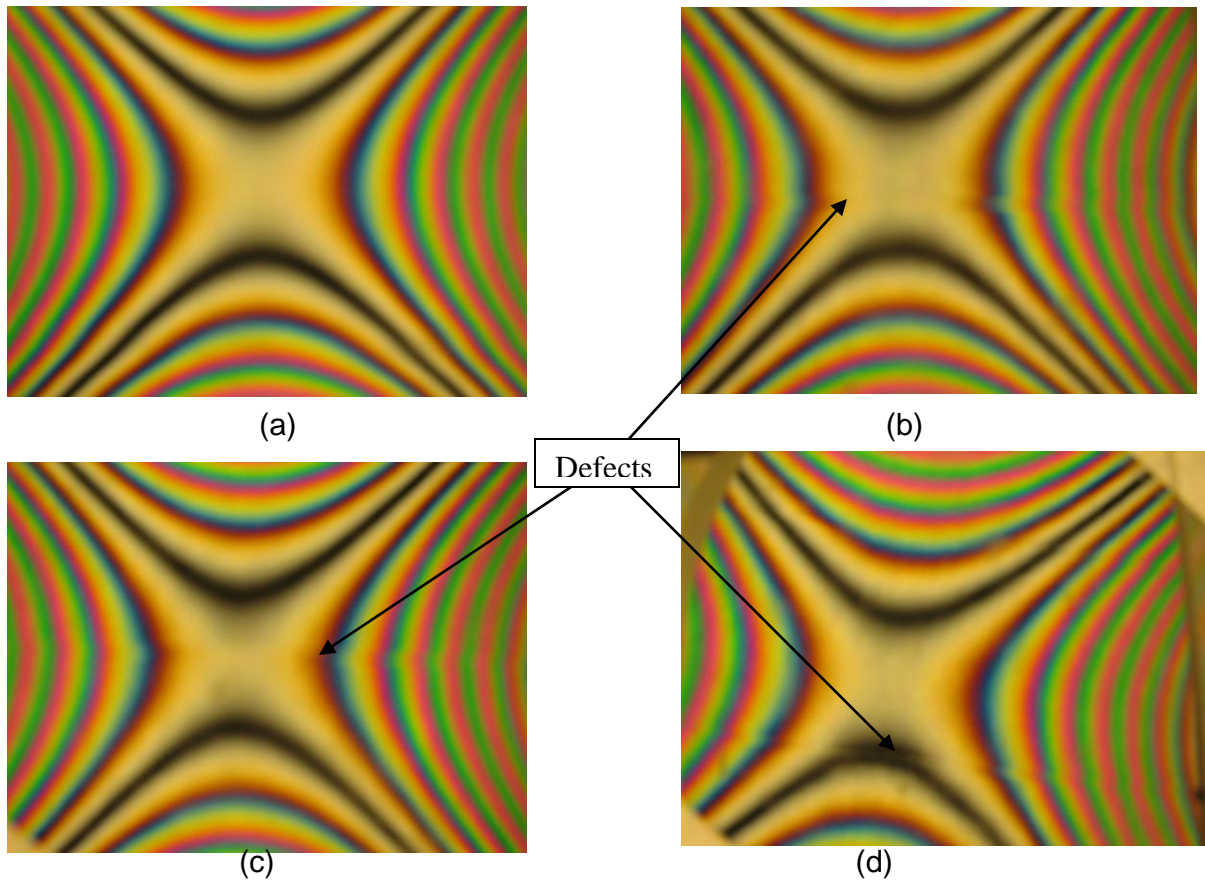


Figure 12. Photoelastic fringe patterns showing the distribution of stress and defects on four different sapphire panels in an inspection-polished condition prior to EEO optical fabrication.

3.0 Future Needs

In general, a more complete understanding of the relationships between the degree of polarization/birefringence, coloration, and induced strain will lead to the development of a viable stress/defect characterization method. More specifically, one of the main impediments in the application of the modified polariscope for quantitative stress analysis is the difficulty in accurately determining the relative retardation or fringe order. The analysis process and data interpretation are time-consuming and observer-dependent. Automated analysis of full-field photoelastic data with little or no operator interaction would overcome these problems and provide precise, reproducible, and quantitative measurements. More work is required in this area with specific application to sapphire panels.

4.0 Summary

Photoelasticity is a very rapid and cost effective technique for identifying and measuring defects and stresses in large sapphire panels used for optical applications. In this work we developed and demonstrated the utility of this technique by detecting defects and stresses in sapphire panels. Defects, inhomogeneous structures and stress patterns in sapphire panels were clearly revealed. Defect detection shows directional dependence on the crystal axes. The defects are mostly affected by the application of induced stress. Observation of a stress gradient across the panel suggests that atomic motion is parallel to the direction of uniaxial compression. Incorporation of an

additional birefringent plate in the conventional circular polariscope considerably improved the sensitivity of defect detection. Qualitative analysis of stress concentration points and stress regions and other defects associated with growth and fabrication operations can be identified easily. The information can be used as an on-line check for sapphire quality inspection and process improvement. This technique offers an excellent inspection capability for detection of a wide variety of defect types, and has the potential to serve as a quantitative tool for characterizing stress in sapphire panels. The fact that large panels can be characterized quickly in a single view renders this method especially attractive as a simple shop-floor tool for revealing internal stresses.

Acknowledgement

This work was sponsored by the Office of the Naval Research (ONR) under Contract No. N00014-04-C-0419, and Air Force Research Laboratory (AFRL) under Contracts No. FA 8650-05-D-5806/0004 and No. FA 8650-06-5401/006.

References:

1. J.E. Greivenkamp, M. T. Chang, in *Optical fabrication and testing workshop*, 1992 Technical Digest Series, **24**, (OSA, Washington, DC 1992).L. Grabner, J. Appl. Phys., **49** (2) 580-83 (1978).
2. D. Harris, *Materials for Infrared Windows and Domes: Properties and Performance*, SPIE, Bellingham, WA, (1998).
3. Y. Zhou, P. D. Funkenbusch, D. J. Quesnel, D. Golini and A. Lindquist, J. Am. Ceram. Soc. **77** (12) 3277-80 (1994).